LEARNING PERTURBATION EFFECTS THROUGH CONTRASTIVE ALIGNMENT OF TRANSCRIPTOMICS AND TEXTUAL EMBEDDINGS

Anonymous authors
Paper under double-blind review

ABSTRACT

Single-cell perturbation screens offer a scalable approach for characterizing the effects of genetic and chemical interventions on cellular state. However, most existing representation-learning methods are tailored to a single perturbation modality and fail to explicitly incorporate external semantic knowledge, which limits their ability to generalize across datasets and perturbation types. Here, we introduce PertOmni, a CLIP-style multimodal representation-learning framework that aligns transcriptomic perturbation signatures with text-derived embeddings of curated gene and compound descriptions. PertOmni jointly trains a shared transcriptomic encoder and dataset-specific text encoders using a masked contrastive objective that emphasizes within–cell-type discrimination while mitigating confounding effects arising from cell-type heterogeneity. We evaluate the produced joint embedding space on bi-directional retrieval, drug–gene interaction inference, and perturbation prediction across both small-molecule and CRISPRi perturbation datasets, and demonstrate consistent improvements over strong baseline methods.

1 INTRODUCTION

Numerous perturbation experiments have been developed to systematically quantify cellular changes under varying conditions (Datlinger et al., 2017; Dixit et al., 2016; Jaitin et al., 2016; Gilbert et al., 2014), enabling the study of how cells respond to interventions. Recent advances in single-cell RNA sequencing enable these responses to be profiled at single-cell resolution, yielding control and perturbed transcriptomic readouts across many perturbations (Dixit et al., 2016; Adamson et al., 2016; Peidli et al., 2024). Broadly speaking, such perturbations can be categorized into three major categories based on the perturbagen used. Genetic perturbations, such as CRISPR-based ones (Dixit et al., 2016), leverage targeted genome editing to disrupt or modulate gene function, thereby altering the expression of the perturbed gene and its associated regulatory network. Small-molecule perturbations (Srivatsan et al., 2020; Zhang et al., 2025), in contrast, use chemical compounds that typically act on protein products such as enzymes or receptors, indirectly reshaping the transcriptional landscape of affected pathways. Biologics form another category and include, for example, extracellular ligand stimulation with cytokines. Together, these experimental strategies have become important tools for understanding cellular circuitry, providing insights into fundamental biology and enabling the discovery of therapeutic targets.

Analyzing gene expression profiles from perturbation experiments remains challenging. Historically, the high cost of such experiments limited the availability of large-scale, genome-wide, or atlas-level datasets (Peidli et al., 2024). Although several institutes and companies have released single-cell perturbation datasets with multiple replicates and experimental conditions (Zhang et al., 2025; Nadig et al., 2025; Szałata et al., 2024a; DeMeo et al., 2025), data quality and noise remain persistent concerns. Perturbations can trigger stress or cell-death programs; moreover, nuclease-based genetic perturbations can induce complex DNA damage such as chromothripsis (Leibowitz et al., 2021), and perturbation efficacy can be heterogeneous across cells (Jiang et al., 2025). In addition, single-cell RNA-seq measurements are prone to technical artifacts and batch effects (Tung et al., 2017; Long et al., 2025). These challenges present as obstacles in analyzing perturbation effects rigorously.

A range of computational methods for denoising, normalizing, and modeling perturbation responses has been proposed to address these challenges, including Hetzel et al. (2022); Roohani et al. (2024); Piran et al. (2024); Wang et al. (2024); Klein et al. (2025); Adduri et al. (2025); Liu et al. (2026). These methods typically use as input a representation of the perturbagen and the transcriptomic profile of the control cells of interest. More recently, several single-cell foundation models such as Cui et al. (2024); Hao et al. (2024); Theodoris et al. (2023); Szałata et al. (2024b) have also claimed to support perturbation response prediction, but benchmarking studies such as Liu et al. (2023); Kedzierska et al. (2025); Szałata et al. (2024a) suggest that their generalization remains limited. scGen (Lotfollahi et al., 2019) aims to predict single-cell perturbation responses by learning a latent representation and transferring perturbation effects via latent-space arithmetic, while GPerturb (Xing & Yau, 2025) estimates gene-level perturbation effects with calibrated uncertainty. Despite these advances, two major gaps remain. First, most approaches overlook the integration of external biological knowledge expressed in natural language, such as functional annotations of genes and drugs, which could improve interpretability and predictive accuracy. Second, few frameworks model both genetic and chemical perturbations. Such integration would enable the inference of drug–target relationships.

Therefore, we introduce PertOmni, a unified framework for modeling and bridging perturbation data across diverse perturbagens and technologies. PertOmni learns a shared embedding space by contrastively aligning LLM-derived perturbation text embeddings with transcriptomic perturbation-effect embeddings across genetic and small-molecule screens. Specifically, we embed curated gene and drug descriptions, such as from NCBI (Schoch et al., 2020), and jointly train text and transcriptome encoders so that matched perturbations and expression readout are close in the latent space. We evaluate PertOmni on (i) bi-directional perturbation retrieval (text to transcriptome and transcriptome to text) and (ii) downstream applications, including drug–gene interaction inference and retrieval-based perturbation prediction, demonstrating improved alignment and utility compared to strong baselines. Codes of PertOmni can be found here [1].

2 METHODS

Problem definition. Our objective is to learn aligned representations of perturbation effects from single-cell transcriptomic perturbation data and LLM embeddings. Consider a perturbation dataset $\mathcal{D} = \{(x_i, p_i, c_i)\}_{i=1}^{N}$, where $x_i \in \mathbb{R}^G$ is the pseudobulk expression vector for sample i, p_i denotes the perturbation condition (gene knockdown or small molecule), and c_i denotes the corresponding cell line. We learn a transcriptome encoder P^X and text encoders P^Z that map inputs to a shared embedding space:

$$E_i = P^X(x_i), \qquad Z_i = P^Z([\mathrm{LLM}(p_{\text{text},i}); \mathrm{LLM}(c_{\text{text},i})]) \tag{1}$$

where $p_{\text{text},i}$ and $c_{\text{text},i}$ are textual descriptions of the perturbation and cell line for sample i, respectively, $\mathrm{LLM}(\cdot)$ denotes a fixed text embedding model, $[\cdot;\cdot]$ denotes concatenation, and $E_i, Z_i \in \mathbb{R}^d$. We demonstrate that the learned transcriptome embeddings (E) and text embeddings (Z) support multiple downstream applications via linear probing or joint fine-tuning.

Data preparation. For small-molecule perturbations, we use the Tahoe-100M dataset (Zhang et al., 2025). For genetic perturbations, we use 5 cell lines across 3 datasets: K562 and RPE1 (Replogle et al., 2022), HepG2 and Jurkat (Nadig et al., 2025), and HCT116 (Huang et al., 2025). For both modalities, cells and genes are first filtered based on standard quality control criteria following the Scanpy tutorial (Wolf et al., 2018), including the removal of cells that express fewer than 100 genes and the removal of genes that are detected in fewer than three cells. In each plate or batch, we perform pseudobulk aggregation by summing gene expression across cells sharing the same condition (perturbation and cell line). Then, normalization is performed following the Scanpy tutorial (Wolf et al., 2018), where we count-normalize each pseudobulk sample to the median of total counts and apply a log1p transformation. For the Tahoe-100M dataset, text descriptions for perturbations are obtained directly from the dataset, where compound descriptions are extracted from MedChemExpress (MedChemExpress) using Selenium(Selenium Contributers). For CRISPRi data, embeddings for target genes are taken from GenePT (Chen & Zou, 2025). For both datasets, cell line text descriptions are generated from GPT-4o using the prompt: ”Please summarize the information of cell

[1] Codebase: `https://anonymous.4open.science/r/PertOmni-D728/`

line: {cell line} in one paragraph. Use academic language and include pathway information." All perturbation- and cell line-level text descriptions are then converted into 1536-dimensional embeddings using the text-embedding-3-small model.

We split the training, validation, and test sets based on perturbations in the two datasets, ensuring that perturbations in the test set are not observed during training. For PertOmni-chem and PertOmni-cri training, we use all genes in Tahoe-100M dataset and CRISPRi dataset, respectively. For PertOmni training, we use the intersection of genes between the two datasets.

Encoder architecture. All encoders (P^X, P^Z_d, P^Z_g) are lightweight projection heads with two fully-connected layers and a residual connection. Each maps an input of dimension d to a 128-dimensional latent: a linear layer to 128 dimensions, GELU, a second 128 × 128 linear layer with dropout, residual addition to the first projection, and layer normalization.

Masked contrastive learning. Our model follows Contrastive Language-Image Pre-Training (CLIP) (Radford et al., 2021) and its sigmoid-based variant SigLIP (Zhai et al., 2023), aligning paired samples across modalities by increasing similarity of matched pairs and decreasing similarity of unmatched pairs. In our setting, each sample consists of a gene expression profile paired with LLM-derived embeddings of the perturbation and cell line.

We encode gene expression with a shared transcriptome encoder P^X. We encode text with modality-specific text encoders: P^Z_d for small-molecule data and P^Z_g for genetic perturbation data. Each text encoder takes as input the concatenation of perturbation and cell-line text embeddings. For genetic perturbation data, we additionally concatenate LLM-derived embeddings of Gene Ontology biological pathways related to each target gene, where pathway descriptions are obtained from MSigDB (Subramanian et al., 2005; Liberzon et al., 2015). We train P^X jointly with P^Z_d and P^Z_g using a contrastive objective, and share the weights of the final fully-connected layer between P^Z_d and P^Z_g to encourage alignment across perturbation types. The architecture is visualized in Figure 1(a). We denote text embeddings for chemical perturbations as T and for genetic perturbations as M.

Let the small-molecule and genetic perturbation datasets contain n and m samples, respectively. Let x_i denote the input gene expression vector for sample i, and let $c_{\text{text}}, p_{\text{text}}$ be text descriptions of the cell line and perturbation. For the small-molecule perturbation dataset, we encode embeddings from the encoders as $E_i = P^X(x_i)$ and $T_i = P^Z_d([\text{LLM}(p_{\text{text},i}); \text{LLM}(c_{\text{text},i})])$ for the i_{th} sample. For the genetic perturbation dataset, encoded embeddings are $E_{i'} = P^X(x'_{i'})$ and $M_{i'} = P^Z_g([\text{LLM}(p_{\text{text},i'}); \text{LLM}(c_{\text{text},i'})])$ for the i'th sample. Our loss function is written as:

$$L_{mCLIP} = -\frac{1}{n}\sum_{i,j} \log \sigma(Y_{ij} \cdot \langle E_i, T_j \rangle / t) - \frac{1}{m}\sum_{i',j'} \log \sigma(Y_{i'j'} \cdot \langle E_{i'}, M_{j'} \rangle / t) \tag{2}$$

where t is temperature, $Y_{ij}, Y_{i'j'}$ specify how each cross-modal pair contributes to the contrastive objective (positive, negative, or masked), and $\langle \cdot, \cdot \rangle$ denotes cosine similarity. σ is the sigmoid function.

In standard SigLIP, $Y_{ij} = +1$ if E_i and T_j correspond to the same sample (matched pair) and $Y_{ij} = -1$ otherwise (unmatched pair). In our setting, we perform contrastive learning only within cell lines. Concretely, we mask all pairs across different cell lines so that they do not contribute to the loss:

$$Y_{ij} = \begin{cases} +1 & \text{if } i = j \text{ (matched pair)} \\ -1 & \text{if } i \neq j \text{ and } c_i = c_j \text{ (within-cell-line negative)} \\ 0 & \text{if } c_i \neq c_j \text{ (masked)} \end{cases} \tag{3}$$

(and analogously for $Y_{i'j'}$ in the genetic perturbation dataset). Here, c_i denotes the discrete cell-line identity label used for masking. A visualization of Y is shown in Figure 1(b). Hyperparameters are described in Table 1.

Cross–cell-line negatives in standard contrastive learning can encourage the model to separate samples primarily by cell identity rather than perturbation identity, because baseline expression programs differ strongly across contexts. By setting $Y_{ij} = 0$ when $c_i \neq c_j$ (Eq. (3)), we prevent the objective from using cell line as an easy shortcut and instead force discrimination among perturbations within the same context. This design makes the learned space well-suited for context-conditional

Hyperparameter	Value
Minimum epochs	100
Learning rate	1.0×10^{-4}
Tahoe-side temperature	5
CRISPR-side temperature	5

Table 1: Training hyperparameters. Temperatures correspond to the scaling factor t in Eq. (2) for Tahoe (chemical) and CRISPR (genetic) datasets. Details of experiment settings are shown in Appendix A. Hyperparameter sensitivity is shown in Supplementary Figures.

tasks (e.g., retrieval and kNN prediction within a given cell line), at the cost of not explicitly enforcing that a perturbation's embedding be invariant across cell lines. In joint training, cross-context generalization can still emerge indirectly through shared encoder parameters and shared perturbation text priors, but we do not assume perturbation effects are globally comparable across cell types.

Perturbation retrieval. Using the learned transcriptome and text embeddings from PertOmni, we perform intra-cell-line retrieval between different modalities based on cosine similarity. For this task, we evaluate retrieval performance using three retrieval metrics shown below:

Let Q be a set of queries. For each query $q \in Q$, let g_q be the ground-truth target and $R_q = (r_{q,1}, \ldots, r_{q,N})$ be the ranked list of retrieved items. Define $rank_q = \min\{i \in \{1, \ldots, N\} \mid r_{q,i} = g_q\}$.

1. Accuracy score for top-K retrieval measures whether the ground truth appears within the retrieved candidates. It is defined as

$$acc@topK = \frac{1}{|Q|} \sum_{q \in Q} \mathbb{I}[rank_q \leq K]. \tag{4}$$

2. Normalized discounted cumulative gain (nDCG) score for top-K retrieval measures overall ranking quality. It is defined as

$$nDCG@topK = \frac{1}{|Q|} \sum_{q \in Q} \mathbb{I}[rank_q \leq K] \frac{1}{\log_2(rank_q + 1)} \tag{5}$$

3. Mean reciprocal rank (MRR) score captures how early the ground-truth target appears in the ranked list. It is defined as

$$mrr = \frac{1}{|Q|} \sum_{q \in Q} \frac{1}{rank_q} \tag{6}$$

Gene-drug interaction prediction. This task aims to identify target genes for chemical perturbations (Drug2Gene) and identify chemicals that target a specific gene (Gene2Drug). We fine-tune PertOmni using interaction annotations from DGIdb (Cannon et al., 2024). Since DGIdb is incomplete, the absence of an annotation does not imply a true negative interaction. We therefore treat this as a positive–unlabeled learning problem and optimize a positive-only objective: annotated drug–gene pairs are encouraged to have high similarity in the learned embedding space, while unannotated pairs are ignored during the development process.

Let $A_{ij} \in \{0, 1\}$ denote whether DGIdb annotates an interaction between drug i and gene j, and let $s_{ij} = \langle T_i, M_j \rangle / t$ be the scaled cosine similarity between the corresponding embeddings. To train the model, we optimize the following objective:

$$L_{ft} = -\frac{1}{|\mathcal{P}|} \sum_{(i,j) \in \mathcal{P}} \log \sigma(s_{ij}), \quad \mathcal{P} = \{(i,j) : A_{ij} = 1\}, \tag{7}$$

where T_i and M_j are outputs from the drug and gene text encoders of PertOmni, respectively.

For this task (PertOmni$_{ft}$), we initialize from the pretrained PertOmni model and optimize only the dataset-specific text encoders (P_d^Z, P_g^Z) under Eq. (7), while keeping the shared transcriptome encoder (P^X) fixed.

Inspired by Chen et al. (2024), we also consider training a Siamese neural network (SNN) on transcriptomic, text, and all (transcriptomic+text) embedding as a strong baseline for comparison. The SNN applies shared weights to a pair of drug and gene embeddings, followed by element-wise multiplication of the resulting representations and a classifier that predicts the probability of a drug-gene pairing. Following Chen et al. (2024), we apply a balanced training strategy to prevent the SNN from being biased towards well-known targets. Specifically, for the Drug2Gene task, for each gene in a positive pair, we sample a drug that is not annotated to target that gene to form an unannotated contrast pair; for the Gene2Drug task, the other way round.

For evaluation, we use AUROC and AUPRC as metrics, since this is a binary classification problem for each drug-gene pair. Here we treat unannotated pairs as negatives, noting this likely underestimates performance due to label incompleteness.

Perturbation prediction. Inspired by LangPert (Märtens et al.), we perform retrieval between text embedding in the testing set and text or transcriptome embedding in the training set, followed by k-nearest neighbors (kNN) aggregation of retrieved training samples' expression profiles to generate predictions. Additionally, we first use retrieval to narrow down candidate perturbations, then use the refined LangPert model to obtain the final prediction. Model performance is evaluated using Pearson correlation between predicted and observed gene expression, computed over all genes or the top 20 differentially expressed genes (DEGs).

Transcriptomic embedding ablations. We perform an ablation study to evaluate alternative methods for embedding transcriptomic profiles. Either pseudobulk or embeddings are then used as input x to the transcriptome encoder P^X in PertOmni. The evaluation uses cross-modality retrieval as a metric. We compare PertOmni directly on pseudobulk with two foundation-model baselines: scGPT (Cui et al., 2024) and PaSCient (Liu et al., 2025). We generate cell-level embeddings using scGPT, then aggregate them to the sample level, whereas PaSCient directly generates sample-level embeddings. In addition, we test random matching and one-hot embeddings in place of the LLM-derived perturbation and cell line embeddings. Training cost comparisons are presented in Supplementary Table 4.

3 Results

Method overview. Figure 1 summarizes PertOmni, which learns a joint embedding space aligning (i) perturbed transcriptomic profiles and (ii) perturbation identities across genetic and small-molecule screens. PertOmni uses a shared transcriptome encoder and perturbation-type–specific text encoders (gene vs compound) that map LLM-initialized textual descriptions into the same latent space. Training uses a masked contrastive objective that forms negatives only within the same cell line, reducing confounding from cross–cell-line heterogeneity while preserving fine-grained within-context discrimination.

We evaluate the learned embeddings on three downstream uses: (i) drug–gene interaction inference (Chen et al., 2024) via fine-tuning the text encoders on DGIdb labels (Figure 2), (ii) retrieval-based perturbation effect prediction using nearest neighbors in the learned space (Figure 3), (iii) bi-directional cross-modality retrieval between text and transcriptome embeddings (Figure 4). Additional ablations on transcriptome embedding choices are in Supplementary Figure 4.

Predicting drug–gene interaction with PertOmni. We fine-tune PertOmni for drug–gene interaction inference by optimizing a retrieval-style objective that increases similarity for annotated DGIdb drug–gene pairs while leaving unannotated pairs untreated (positive–unlabeled setting). We split drugs and genes so that test drugs/genes are unseen during training, and evaluate two settings: Drug2Gene (rank genes for a drug) and Gene2Drug (rank drugs for a gene). Baselines include similarity-based matching (TahoeBlog), and an SNN classifier trained on Vision Scores (DeTomaso et al., 2019) or PertOmni text, transcriptome, or text+transcriptome embeddings.

As shown in Figure 2(a–d), *PertOmni_ft+text* achieves the best performance across both tasks, improving AUROC and AUPRC over all similarity-based baselines and over the SNN classifier. Supplementary Fig. 3 shows that fine-tuning substantially improves over the zero-shot variant, indicating that aligning embeddings with interaction supervision is important beyond generic retrieval alignment.

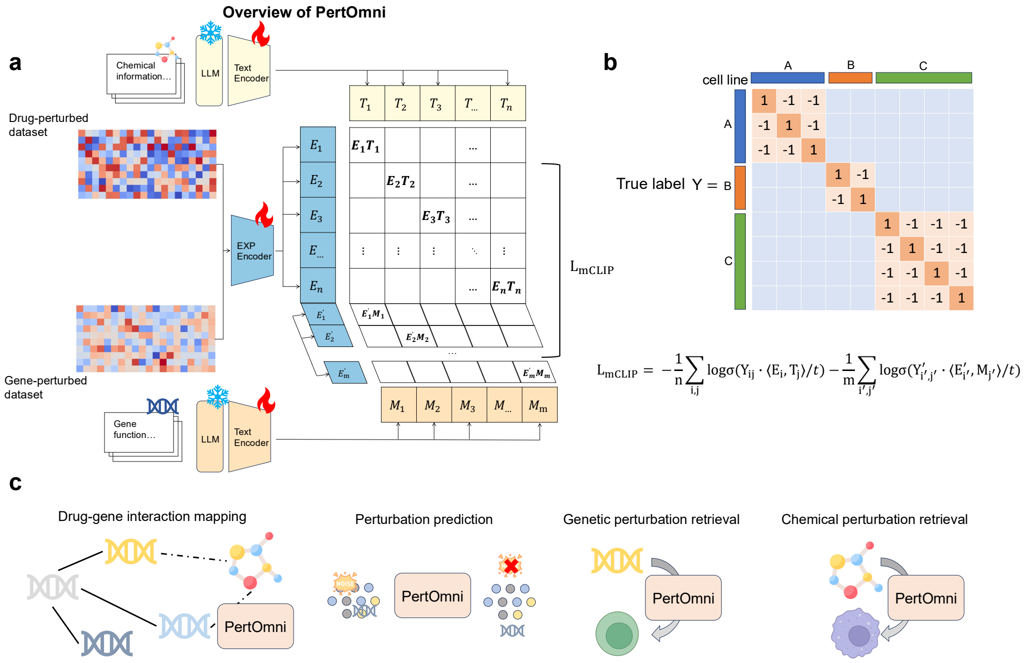
Overview of PertOmni
a
Chemical information...
LLM
Text Encoder
Drug-perturbed dataset
EXP Encoder
Gene-perturbed dataset
Gene function...
T_1 T_2 T_3 $T_{...}$ T_n
E_1 E_2 E_3 $E_{...}$ E_n
E_1T_1 E_2T_2 E_3T_3 E_nT_n
E'_1M_1 E'_2M_2 E'_mM_m
M_1 M_2 M_3 $M_{...}$ M_m
L_{mCLIP}
b
cell line
A
B
C
True label Y =
$L_{mCLIP} = -\frac{1}{n}\sum_{i,j} \log\sigma(Y_{ij} \cdot \langle E_i, T_j\rangle/t) - \frac{1}{m}\sum_{i',j'} \log\sigma(Y'_{i',j'} \cdot \langle E'_{i'}, M_{j'}\rangle/t)$
c
Drug-gene interaction mapping
Perturbation prediction
Genetic perturbation retrieval
Chemical perturbation retrieval
PertOmni

Figure 1: Overview of PertOmni. (a) The illustration of the model architecture. We leverage contrastive learning and modality-specific encoders to build PertOmni. (b) The illustration of masked contrastive learning. We modify the CLIP loss, L_{mCLIP}, to leverage multimodal and masked information during training. (c) Task illustration of downstream applications.

Because DGIdb annotations are sparse, we report AUPRC alongside the task positive rate and interpret gains relative to this baseline. Drug2Gene is consistently harder than Gene2Drug, consistent with the many-to-many nature of drug targeting and incomplete interaction annotations: a single compound can have multiple true targets, and many true targets may be unlabeled.

Predicting perturbation effects with PertOmni. We evaluate retrieval-based perturbation prediction by querying the learned embedding space for nearest-neighbor perturbations and aggregating their observed expression profiles to predict the held-out perturbation response. Unlike LLM-only approaches such as LangPert (Märtens et al.), PertOmni provides an explicit, data-grounded neighborhood over perturbations that can be used directly for kNN prediction and for defining gene sets.

Figure 3(a–f) reports Pearson correlation between predicted and observed expression across three perturb-seq datasets (RPE1 (Nadig et al., 2025), HepG2, Jurkat (Replogle et al., 2022)), evaluated on either all genes or the top-20 DEGs. Across settings, kNN prediction using PertOmni text embeddings yields the best performance, though performance is sensitive to the neighborhood size k. At larger k, transcriptome-derived embeddings become competitive with text embeddings, suggesting that denser neighborhoods partially compensate for weaker semantic priors. PertOmni consistently outperforms LangPert when evaluated on sufficiently large gene sets; moreover, LangPert improves when restricted to gene sets proposed by PertOmni, indicating that the gene-selection signal learned by PertOmni is useful beyond our framework. We include the non-control (non-ctrl) mean as a strong baseline. While competitive at small k, this baseline is consistently surpassed by PertOmni as k increases, whereas other methods, including LangPert, do not reliably outperform it.

Cross-modality retrieval benchmarking. We assess how well PertOmni aligns transcriptomic and textual representations using bi-directional retrieval (text↔transcriptome) under two perturbation regimes: chemical-only training on Tahoe-100M (Zhang et al., 2025), CRISPRi-only training on merged perturb-seq datasets (Replogle et al., 2022; Nadig et al., 2025; Huang et al., 2025), and joint training on both. We compare against single-modality baselines (e.g., scGPT (Cui et al., 2024), PaSCient (Liu et al., 2025)), one-hot embeddings, and random matching. Retrieval is evaluated with ACC@K, nDCG@K, MRR, and an aggregate mean score.

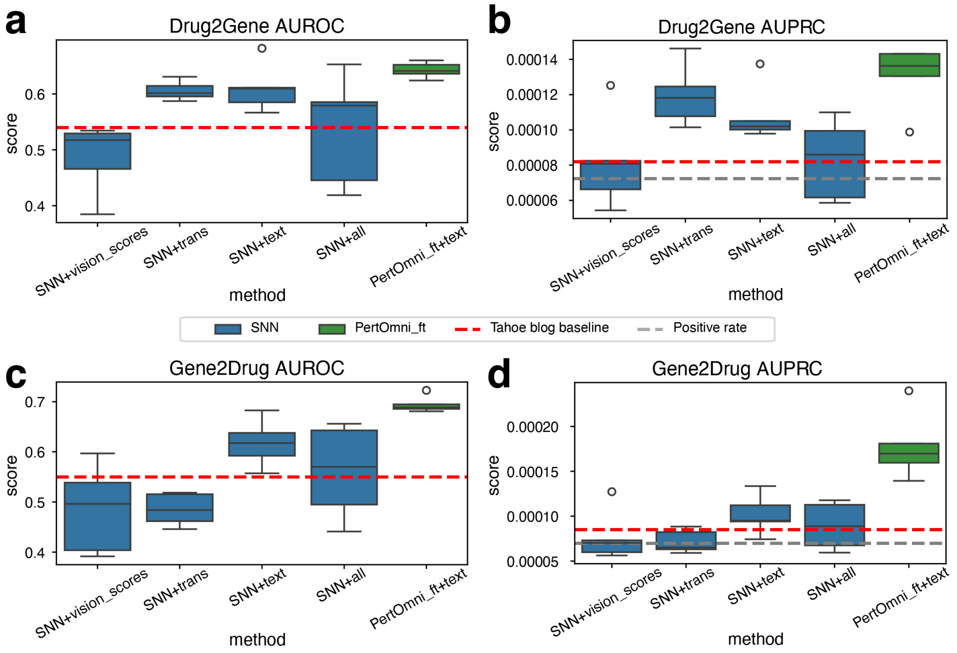

Figure 2: Results of drug-gene pair prediction. Details of choices are summarized in the legend. Tahoe blog baseline first computes differential Vision Scores relative to control cells, and then predicts drug-gene matching using cosine similarity between differential Vision Scores of drugs and genes. (a) AUROC comparison for the Drug2Gene task. (b) AUPRC comparison for the Drug2Gene task. (c) AUROC comparison for the Gene2Drug task. (d) AUPRC comparison for the Gene2Drug task.

Figure 4 summarizes performance with a bubble plot across metrics. PertOmni and its variants achieve the top or near-top rank on most metrics in both Tahoe and CRISPR settings, indicating robust cross-modal alignment rather than gains limited to a single modality. Detailed results are in Supplementary Figures 1 and 2.

Joint training improves CRISPR-side retrieval while slightly degrading Tahoe-side retrieval. We hypothesize that this reflects data imbalance, as we have substantially more CRISPR perturbations, which can bias the shared space toward the higher-sample data. Exploring explicit reweighting or balanced batching is a natural next step. Architecture and hyperparameter ablations are reported in Supplementary Figures 6, 4, 5, 7, 8, 9, 10, 11, 12, and 13.

4 Discussion

We introduce PertOmni, a framework for aligning representations of perturbation effects across modalities. By leveraging LLM embeddings and masked contrastive learning, PertOmni successfully integrates heterogeneous cell context and perturbation information, outperforming strong baselines across three applications relevant to drug discovery. Overall, this work shows that LLM-derived priors can be combined with sequencing readouts to learn transferable perturbation representations. Future work could extend PertOmni to additional modalities and update LLM embeddings to improve generalization with larger and more diverse data.

5 Ethics Statement and Acknowledgment

The authors used LLMs to generate fixed text embeddings for model training and editing of the manuscript, such as rephrasing for clarity.

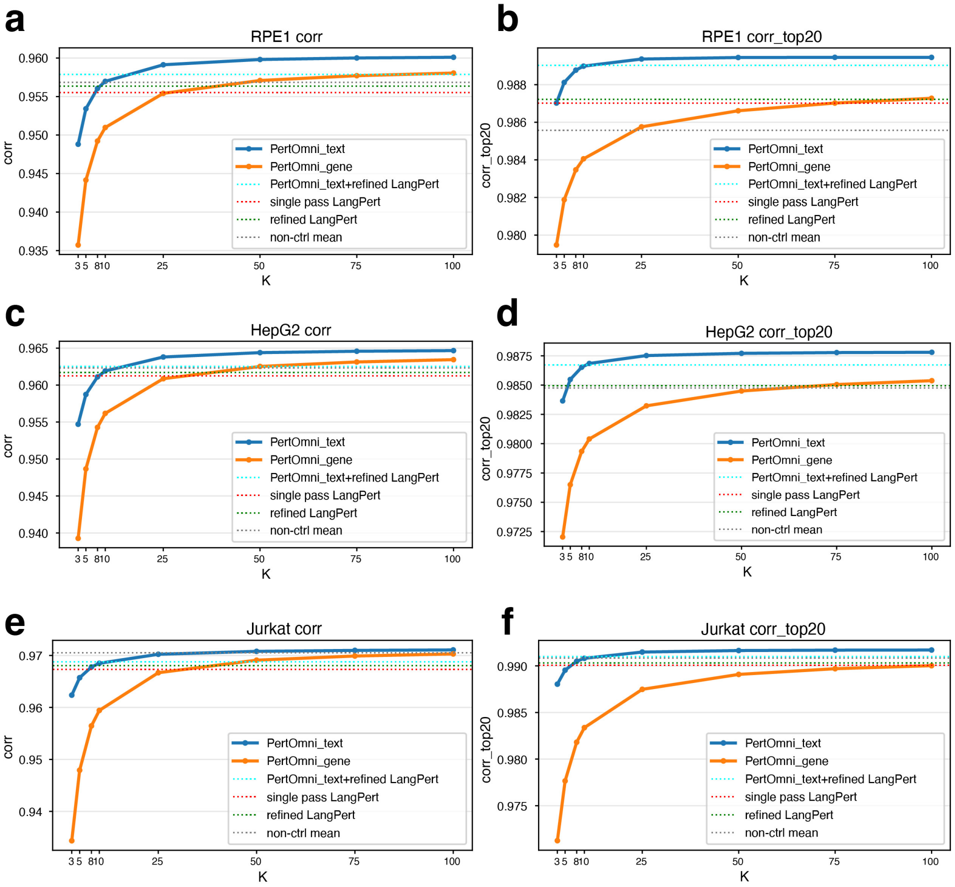

Figure 3: Perturbation prediction via retrieval. Details of methods are summarized in the legend. Performance is measured as the Pearson correlation between predicted and observed gene expression. (a) All genes, RPE1. (b) Top-20 DEGs, RPE1. (c) All genes, HepG2. (d) Top-20 DEGs, HepG2; the red line (single_pass_LangPert) overlaps with the gray line (non-ctrl mean). (e) All genes, Jurkat. (f) Top-20 DEGs, Jurkat.

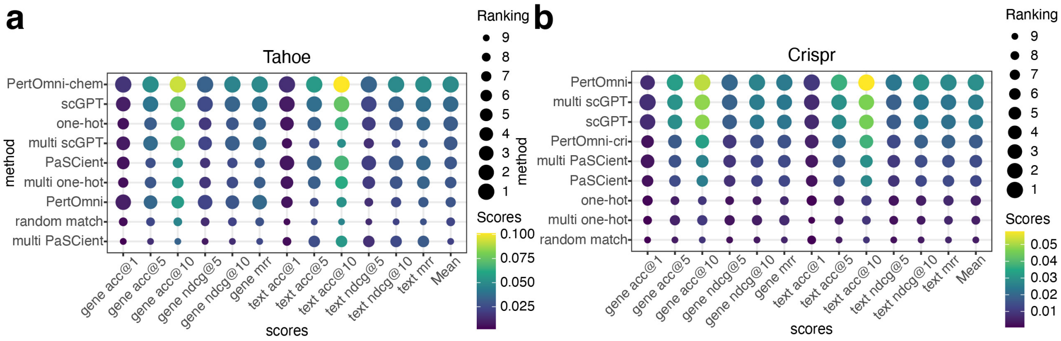

Figure 4: Results of cross-modality retrieval. We find that using training data from two perturbations can benefit CRISPR-based retrieval, whereas it does not improve Chem-based retrieval (Tahoe). (a) Multi-metric comparison based on the Tahoe 100M dataset. (b) Multi-metric comparison based on the merged CRISPR dataset.

REFERENCES

Britt Adamson, Thomas M Norman, Marco Jost, Min Y Cho, James K Nuñez, Yuwen Chen, Jacqueline E Villalta, Luke A Gilbert, Max A Horlbeck, Marco Y Hein, et al. A multiplexed single-cell crispr screening platform enables systematic dissection of the unfolded protein response. *Cell*, 167(7):1867–1882, 2016.

Abhinav K Adduri, Dhruv Gautam, Beatrice Bevilacqua, Alishba Imran, Rohan Shah, Mohsen Naghipourfar, Noam Teyssier, Rajesh Ilango, Sanjay Nagaraj, Mingze Dong, et al. Predicting cellular responses to perturbation across diverse contexts with state. *BioRxiv*, pp. 2025–06, 2025.

Matthew Cannon, James Stevenson, Kathryn Stahl, Rohit Basu, Adam Coffman, Susanna Kiwala, Joshua F McMichael, Kori Kuzma, Dorian Morrissey, Kelsy Cotto, et al. Dgidb 5.0: rebuilding the drug–gene interaction database for precision medicine and drug discovery platforms. *Nucleic Acids Research*, 52(D1):D1227–D1235, 2024.

Hao Chen, Frederick J King, Bin Zhou, Yu Wang, Carter J Canedy, Joel Hayashi, Yang Zhong, Max W Chang, Lars Pache, Julian L Wong, et al. Drug target prediction through deep learning functional representation of gene signatures. *Nature Communications*, 15(1):1853, 2024.

Yiqun Chen and James Zou. Simple and effective embedding model for single-cell biology built from chatgpt. *Nature Biomedical Engineering*, 9(4):483–493, 2025.

Haotian Cui, Chloe Wang, Hassaan Maan, Kuan Pang, Fengning Luo, Nan Duan, and Bo Wang. scgpt: toward building a foundation model for single-cell multi-omics using generative ai. *Nature Methods*, 21(8):1470–1480, 2024.

Paul Datlinger, André F Rendeiro, Christian Schmidl, Thomas Krausgruber, Peter Traxler, Johanna Klughammer, Linda C Schuster, Amelie Kuchler, Donat Alpar, and Christoph Bock. Pooled crispr screening with single-cell transcriptome readout. *Nature Methods*, 14(3):297–301, 2017.

Benjamin DeMeo, Charlotte Nesbitt, Samuel A. Miller, Daniel B. Burkhardt, Inna Lipchina, Doris Fu, Peter Holderrieth, David Kim, Sergey Kolchenko, Artur Szalata, Ishan Gupta, Christine Kerr, Thomas Pfefer, Raziel Rojas-Rodriguez, Sunil Kuppassani, Laurens Kruidenier, Parul B. Doshi, Mahdi Zamanighomi, James J. Collins, Alex K. Shalek, Fabian J. Theis, and Mauricio Cortes. Active learning framework leveraging transcriptomics identifies modulators of disease phenotypes. *Science*, 390(6776):eadi8577, October 2025.

David DeTomaso, Matthew G Jones, Meena Subramaniam, Tal Ashuach, Chun J Ye, and Nir Yosef. Functional interpretation of single cell similarity maps. *Nature Communications*, 10(1):4376, 2019.

Atray Dixit, Oren Parnas, Biyu Li, Jenny Chen, Charles P Fulco, Livnat Jerby-Arnon, Nemanja D Marjanovic, Danielle Dionne, Tyler Burks, Raktima Raychowdhury, et al. Perturb-seq: dissecting molecular circuits with scalable single-cell rna profiling of pooled genetic screens. *Cell*, 167(7): 1853–1866, 2016.

Luke A Gilbert, Max A Horlbeck, Britt Adamson, Jacqueline E Villalta, Yuwen Chen, Evan H Whitehead, Carla Guimaraes, Barbara Panning, Hidde L Ploegh, Michael C Bassik, et al. Genome-scale crispr-mediated control of gene repression and activation. *Cell*, 159(3):647–661, 2014.

Minsheng Hao, Jing Gong, Xin Zeng, Chiming Liu, Yucheng Guo, Xingyi Cheng, Taifeng Wang, Jianzhu Ma, Xuegong Zhang, and Le Song. Large-scale foundation model on single-cell transcriptomics. *Nature Methods*, 21(8):1481–1491, 2024.

Leon Hetzel, Simon Boehm, Niki Kilbertus, Stephan Günnemann, Fabian Theis, et al. Predicting cellular responses to novel drug perturbations at a single-cell resolution. *Advances in Neural Information Processing Systems*, 35:26711–26722, 2022.

Ann C Huang, Tsung-Han S Hsieh, Jiang Zhu, Jackson Michuda, Ashton Teng, Soohong Kim, Elizabeth M Rumsey, Sharon K Lam, Ikenna Anigbogu, Philip Wright, et al. X-atlas/orion: Genome-wide perturb-seq datasets via a scalable fix-cryopreserve platform for training dose-dependent biological foundation models. *BioRxiv*, pp. 2025–06, 2025.

Diego Adhemar Jaitin, Assaf Weiner, Ido Yofe, David Lara-Astiaso, Hadas Keren-Shaul, Eyal David, Tomer Meir Salame, Amos Tanay, Alexander van Oudenaarden, and Ido Amit. Dissecting immune circuits by linking crispr-pooled screens with single-cell rna-seq. *Cell*, 167(7):1883–1896, 2016.

Longda Jiang, Carol Dalgarno, Efthymia Papalexi, Isabella Mascio, Hans-Hermann Wessels, Huiyoung Yun, Nika Iremadze, Gila Lithwick-Yanai, Doron Lipson, and Rahul Satija. Systematic reconstruction of molecular pathway signatures using scalable single-cell perturbation screens. *Nature Cell Biology*, 27(3):505–517, March 2025. ISSN 1476-4679.

Kasia Z Kedzierska, Lorin Crawford, Ava P Amini, and Alex X Lu. Zero-shot evaluation reveals limitations of single-cell foundation models. *Genome Biology*, 26(1):101, 2025.

Dominik Klein, Jonas Simon Fleck, Daniil Bobrovskiy, Lea Zimmermann, Sören Becker, Alessandro Palma, Leander Dony, Alejandro Tejada-Lapuerta, Guillaume Huguet, Hsiu-Chuan Lin, et al. Cellflow enables generative single-cell phenotype modeling with flow matching. *BioRxiv*, pp. 2025–04, 2025.

Mitchell L. Leibowitz, Stamatis Papathanasiou, Phillip A. Doerfler, Logan J. Blaine, Lili Sun, Yu Yao, Cheng-Zhong Zhang, Mitchell J. Weiss, and David Pellman. Chromothripsis as an on-target consequence of CRISPR–Cas9 genome editing. *Nature Genetics*, 53(6):895–905, June 2021. ISSN 1546-1718.

Arthur Liberzon, Chet Birger, Helga Thorvaldsdóttir, Mahmoud Ghandi, Jill P Mesirov, and Pablo Tamayo. The molecular signatures database hallmark gene set collection. *Cell Systems*, 1(6): 417–425, 2015.

Tianyu Liu, Kexing Li, Yuge Wang, Hongyu Li, and Hongyu Zhao. Evaluating the utilities of foundation models in single-cell data analysis. *BioRxiv*, pp. 2023–09, 2023.

Tianyu Liu, Edward De Brouwer, Tony Kuo, Nathaniel Diamant, Alsu Missarova, Hanchen Wang, Minsheng Hao, Hector Corrada Bravo, Gabriele Scalia, Aviv Regev, et al. Learning multi-cellular representations of single-cell transcriptomics data enables characterization of patient-level disease states. In *International Conference on Research in Computational Molecular Biology*, pp. 303–306, 2025.

Tianyu Liu, Tianqi Chen, Wangjie Zheng, Xiao Luo, Yiqun Chen, and Hongyu Zhao. Embeddings from language models are good learners for single-cell data analysis. *Patterns*, pp. 101431, 2026.

Wenxin Long, Tianyu Liu, Lingzhou Xue, and Hongyu Zhao. spvelo: Rna velocity inference for multi-batch spatial transcriptomics data. *Genome Biology*, 26(1):239, 2025.

Mohammad Lotfollahi, F Alexander Wolf, and Fabian J Theis. scgen predicts single-cell perturbation responses. *Nature Methods*, 16(8):715–721, 2019.

Kaspar Märtens, Marc Boubnovski Martell, Cesar A Prada-Medina, and Rory Donovan-Maiye. Langpert: Llm-driven contextual synthesis for unseen perturbation prediction. In *ICLR 2025 Workshop on Machine Learning for Genomics Explorations*.

MedChemExpress. Medchemexpress. URL https://www.medchemexpress.com/. Accessed: 2026-02-04.

Ajay Nadig, Joseph M. Replogle, Angela N. Pogson, Mukundh Murthy, Steven A. McCarroll, Jonathan S. Weissman, Elise B. Robinson, and Luke J. O'Connor. Transcriptome-wide analysis of differential expression in perturbation atlases. *Nature Genetics*, 57(5):1228–1237, May 2025.

Stefan Peidli, Tessa D Green, Ciyue Shen, Torsten Gross, Joseph Min, Samuele Garda, Bo Yuan, Linus J Schumacher, Jake P Taylor-King, Debora S Marks, et al. scperturb: harmonized single-cell perturbation data. *Nature Methods*, 21(3):531–540, 2024.

Zoe Piran, Niv Cohen, Yedid Hoshen, and Mor Nitzan. Disentanglement of single-cell data with biolord. *Nature Biotechnology*, 42(11):1678–1683, 2024.

Alec Radford, Jong Wook Kim, Chris Hallacy, Aditya Ramesh, Gabriel Goh, Sandhini Agarwal, Girish Sastry, Amanda Askell, Pamela Mishkin, Jack Clark, et al. Learning transferable visual models from natural language supervision. In *International Conference on Machine Learning*, pp. 8748–8763. PMLR, 2021.

Joseph M Replogle, Reuben A Saunders, Angela N Pogson, Jeffrey A Hussmann, Alexander Lenail, Alina Guna, Lauren Mascibroda, Eric J Wagner, Karen Adelman, Gila Lithwick-Yanai, et al. Mapping information-rich genotype-phenotype landscapes with genome-scale perturb-seq. *Cell*, 185(14):2559–2575, 2022.

Yusuf Roohani, Kexin Huang, and Jure Leskovec. Predicting transcriptional outcomes of novel multigene perturbations with gears. *Nature Biotechnology*, 42(6):927–935, 2024.

Conrad L Schoch, Stacy Ciufo, Mikhail Domrachev, Carol L Hotton, Sivakumar Kannan, Rogneda Khovanskaya, Detlef Leipe, Richard Mcveigh, Kathleen O'Neill, Barbara Robbertse, et al. Ncbi taxonomy: a comprehensive update on curation, resources and tools. *Database*, 2020:baaa062, 2020.

Selenium Contributers. The selenium project. URL `https://www.selenium.dev/`. Accessed: 2026-02-04.

Sanjay R Srivatsan, José L McFaline-Figueroa, Vijay Ramani, Lauren Saunders, Junyue Cao, Jonathan Packer, Hannah A Pliner, Dana L Jackson, Riza M Daza, Lena Christiansen, et al. Massively multiplex chemical transcriptomics at single-cell resolution. *Science*, 367(6473):45–51, 2020.

Aravind Subramanian, Pablo Tamayo, Vamsi K Mootha, Sayan Mukherjee, Benjamin L Ebert, Michael A Gillette, Amanda Paulovich, Scott L Pomeroy, Todd R Golub, Eric S Lander, et al. Gene set enrichment analysis: a knowledge-based approach for interpreting genome-wide expression profiles. *Proceedings of the National Academy of Sciences*, 102(43):15545–15550, 2005.

Artur Szałata, Andrew Benz, Robrecht Cannoodt, Mauricio Cortes, Jason Fong, Sunil Kuppasani, Richard Lieberman, Tianyu Liu, Javier A. Mas-Rosario, Rico Meinl, Jalil Nourisa, Jared Tumiel, Tin M. Tunjic, Mengbo Wang, Noah Weber, Hongyu Zhao, Benedict Anchang, Fabian J. Theis, Malte D. Luecken, and Daniel B. Burkhardt. A benchmark for prediction of transcriptomic responses to chemical perturbations across cell types. *Advances in Neural Information Processing Systems*, 37:20566–20616, December 2024a.

Artur Szałata, Karin Hrovatin, Sören Becker, Alejandro Tejada-Lapuerta, Haotian Cui, Bo Wang, and Fabian J. Theis. Transformers in single-cell omics: a review and new perspectives. *Nature Methods*, 21(8):1430–1443, August 2024b.

TahoeBlog. Target deconvolution through data integration: Unifying drug and genetic perturbations. `https://blog.tahoebio.ai/p/target-deconvolution-through-data`. Accessed: 2026-01-21.

Christina V Theodoris, Ling Xiao, Anant Chopra, Mark D Chaffin, Zeina R Al Sayed, Matthew C Hill, Helene Mantineo, Elizabeth M Brydon, Zexian Zeng, X Shirley Liu, et al. Transfer learning enables predictions in network biology. *Nature*, 618(7965):616–624, 2023.

Po-Yuan Tung, John D. Blischak, Chiaowen Joyce Hsiao, David A. Knowles, Jonathan E. Burnett, Jonathan K. Pritchard, and Yoav Gilad. Batch effects and the effective design of single-cell gene expression studies. *Scientific Reports*, 7(1):39921, January 2017.

Gefei Wang, Tianyu Liu, Jia Zhao, Youshu Cheng, and Hongyu Zhao. Modeling and predicting single-cell multi-gene perturbation responses with sclambda. *BioRxiv*, 2024.

F Alexander Wolf, Philipp Angerer, and Fabian J Theis. Scanpy: large-scale single-cell gene expression data analysis. *Genome biology*, 19(1):15, 2018.

Hanwen Xing and Christopher Yau. Gperturb: Gaussian process modelling of single-cell perturbation data. *Nature Communications*, 16(1):5423, 2025.

Xiaohua Zhai, Basil Mustafa, Alexander Kolesnikov, and Lucas Beyer. Sigmoid loss for language image pre-training. In *Proceedings of the IEEE/CVF International Conference on Computer Vision*, pp. 11975–11986, 2023.

Jesse Zhang, Airol A Ubas, Richard de Borja, Valentine Svensson, Nicole Thomas, Neha Thakar, Ian Lai, Aidan Winters, Umair Khan, Matthew G Jones, et al. Tahoe-100m: A giga-scale single-cell perturbation atlas for context-dependent gene function and cellular modeling. *BioRxiv*, pp. 2025–02, 2025.

A Experimental settings

For model training, we utilize 128 as batch size, 1e-4 as learning rate, Adam as optimizer, 0.0 as dropout rate, 100 as default epochs, 5.0 as temperature, and top-1 retrieval accuracy as the criteria for early stopping. The choices of hyper parameters satisfy for both cross-modality retrieval and drug-gene interaction prediction tasks.

B Supplementary Tables

Plate	# Samples	# Genes	# Cell Lines	# Perturbations
Plate 1	4516	62710	50	93
Plate 2	4631	62710	50	93
Plate 3	4650	62710	50	93
Plate 4	4750	62710	50	95
Plate 5	4750	62710	50	95
Plate 6	4750	62710	50	95
Plate 7	4700	62710	50	94
Plate 8	4750	62710	50	94
Plate 9	4750	62710	50	94
Plate 10	4750	62710	50	95
Plate 11	4750	62710	50	95
Plate 12	4750	62710	50	95
Plate 13	4700	62710	50	44
Plate 14	4746	62710	50	95
Total	**65943**	**62710**	**50**	**380**

Table 2: Summary statistics of the Tahoe-100M dataset across plates.

Cell Line	# Samples	# Genes	# Cell Lines	# Perturbations
K562	11818	6408	1	9783
RPE1	2373	6408	1	2373
HepG2	2373	6408	1	2373
Jurkat	2373	6408	1	2373
HCT116	18115	6408	1	18115
Total	**37052**	**6408**	**5**	**18385**

Table 3: Summary statistics of the CRISPR perturbation datasets across cell lines.

Tahoe-100M		**CRISPR**		**Multi-dataset**	
Method	Time (s)	Method	Time (s)	Method	Time (s)
PertOmni-chem	2006.02 (18.82)	PertOmni-cri	796.85 (12.00)	PertOmni	2576.25 (19.52)
scGPT	1253.35 (15.69)	scGPT	1244.83 (8.96)	multi scGPT	3301.70 (50.92)
PaSCient	1119.90 (12.85)	PaSCient	1248.61 (16.43)	multi PaSCient	3204.23 (37.16)
one-hot	1988.04 (14.61)	one-hot	657.26 (7.09)	multi one-hot	2364.36 (19.18)

Table 4: Runtime (seconds; mean (std)) on Tahoe-100M, CRISPR, and multi-dataset settings. We use 8 CPUs and 1 NVIDIA RTX 5000 GPU for this experiment.

C Supplementary Figures

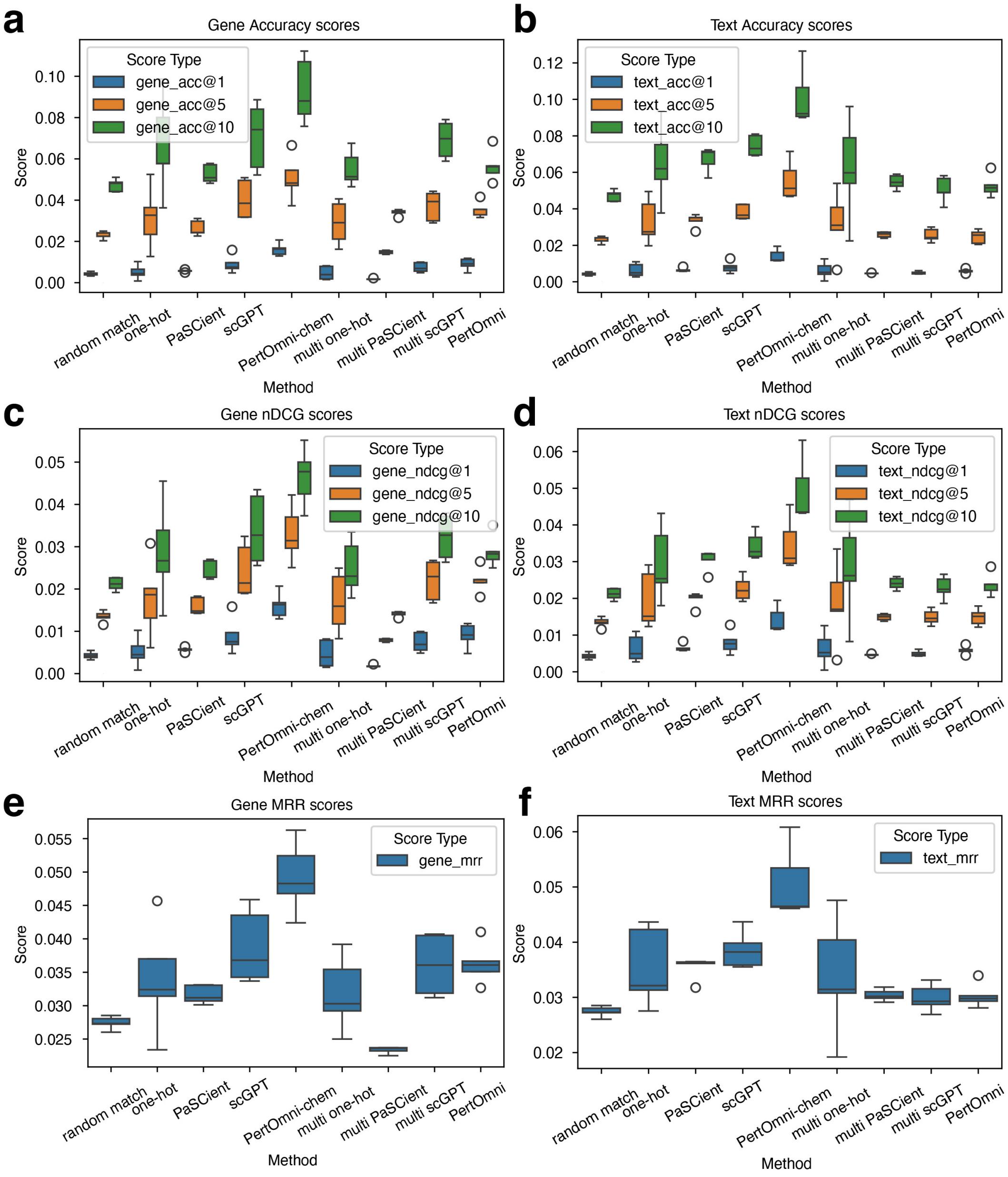

Supplementary Fig. 1: Boxplot visualization of cross-modality retrieval in Tahoe-100m dataset. (a,b) Accuracy retrieval scores comparison. (c,d) nDCG scores comparison. (e,f) MRR scores comparison.

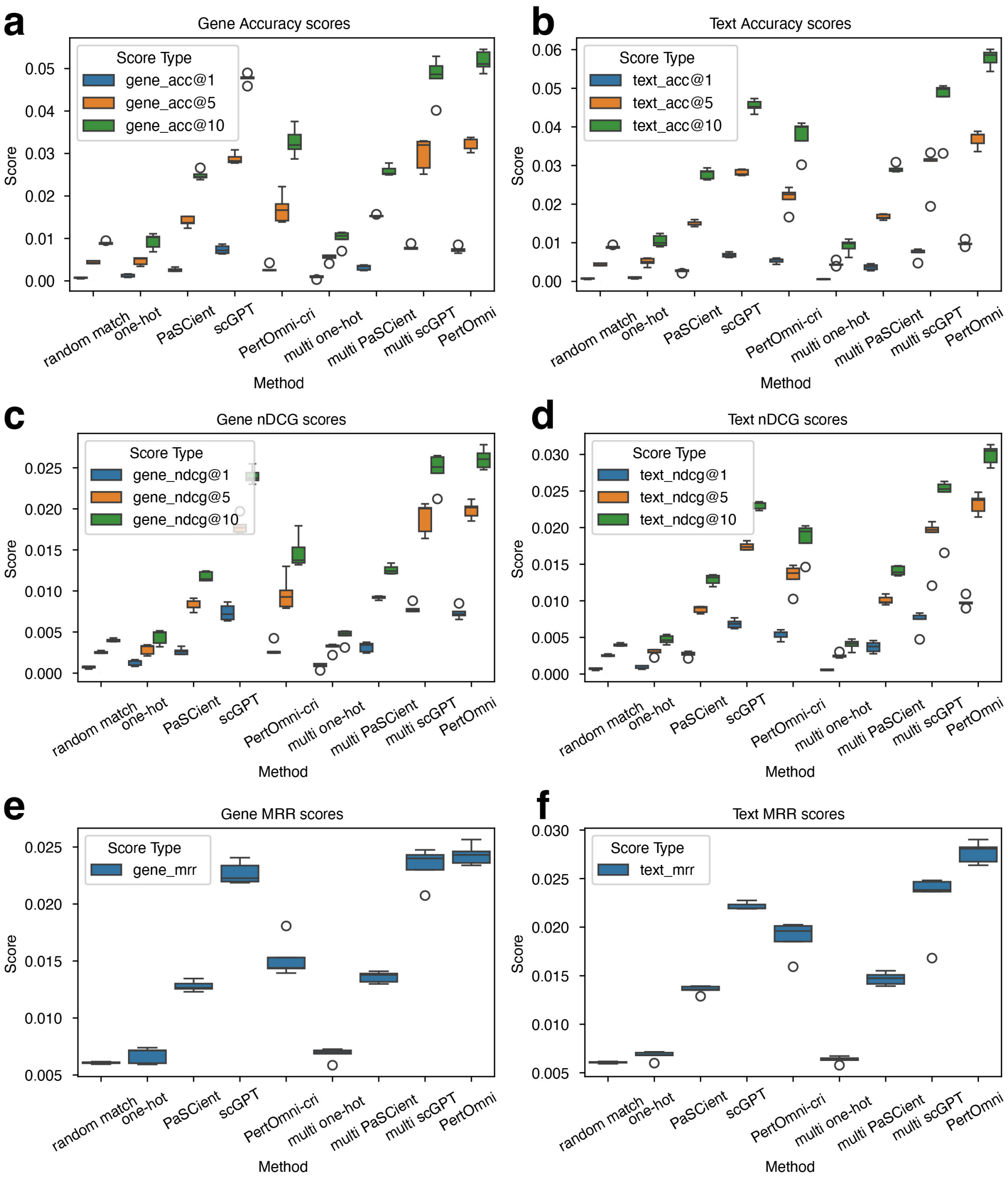

Supplementary Fig. 2: Boxplot visualization of cross-modality retrieval in the CRISPR dataset. (a,b) Accuracy retrieval scores comparison. (c,d) nDCG scores comparison. (e,f) MRR scores comparison.

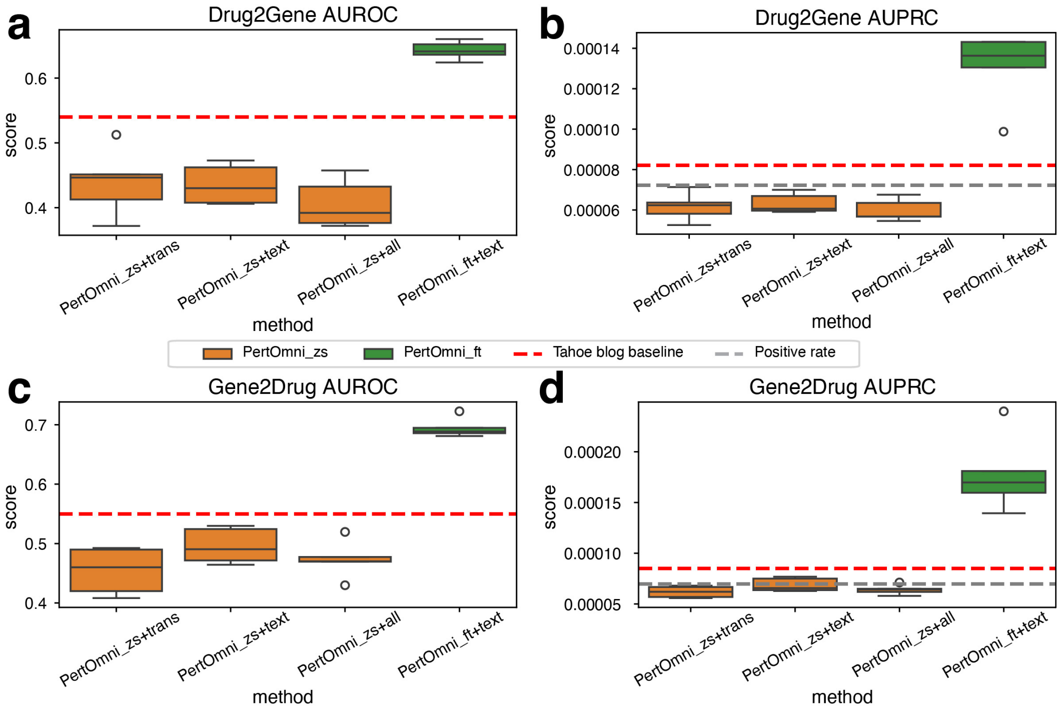

Supplementary Fig. 3: Comparison of drug-gene interaction performance before and after fine-tuning. PertOmni_zs represents the zero-shot performance of PertOmni without training based on paired gene-drug interactions, and PertOmni_ft represents fine-tuned performance. We find that the finetuning (ft) mode performs better. (a) AUROC comparison for the Drug2Gene task. (b) AUPRC comparison for the Drug2Gene task. (c) AUROC comparison for the Gene2Drug task. (d) AUPRC comparison for the Gene2Drug task.

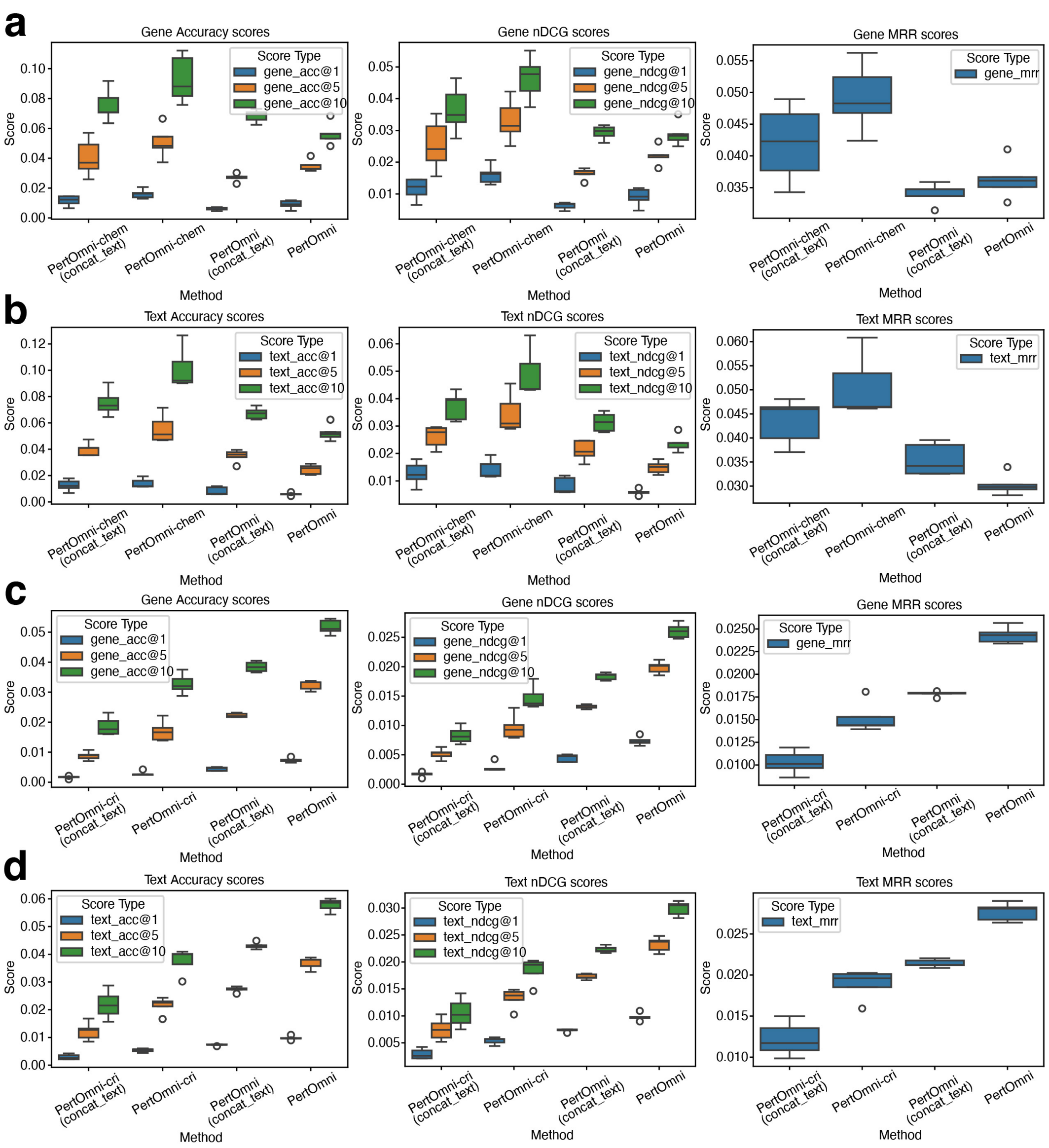

Supplementary Fig. 4: Results of cross-modality retrieval in ablation studies. In this ablation study, we first concatenate text descriptions of perturbation and cell line, and then generate LLM embeddings based on the concatenated descriptions. In contrast, PertOmni first generates LLM embeddings for perturbation and cell line, respectively, and then concatenates LLM embeddings as input to text encoders. (a) Gene2Text retrieval metrics comparison based on the Tahoe-100M dataset. (b) Text2Gene retrieval metrics comparison based on the merged CRISPR dataset.

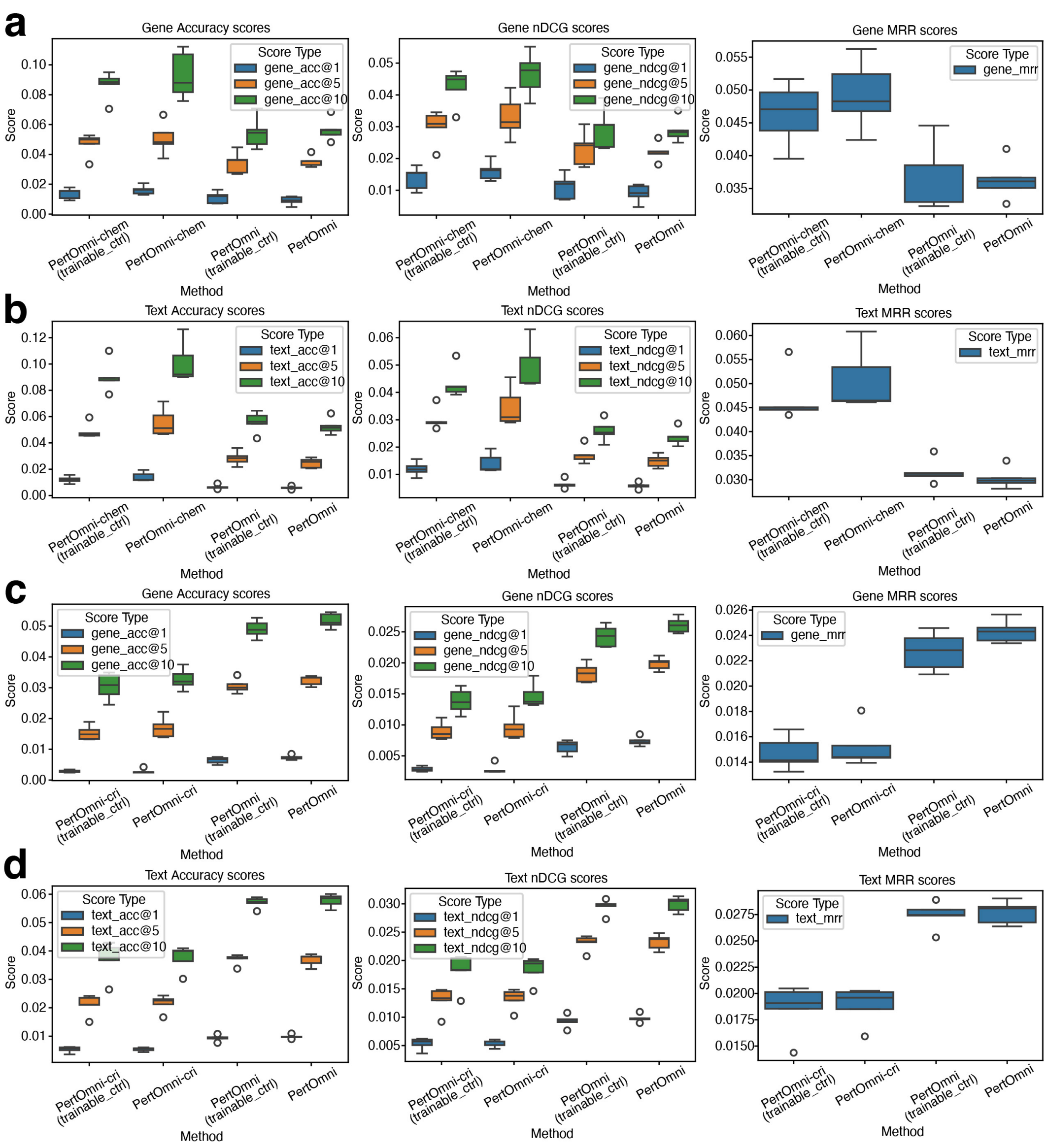

Supplementary Fig. 5: Results of cross-modality retrieval in ablation studies. In this ablation study, we use trainable embedding as input to text encoders for control samples (”DMSO_TF” in Tahoe-100M dataset and ”non-targeting” in CRISPR dataset), instead of using 0s as in PertOmni. (a) Gene2Text retrieval metrics comparison based on the Tahoe-100M dataset. (b) Text2Gene retrieval metrics comparison based on the merged CRISPR dataset.

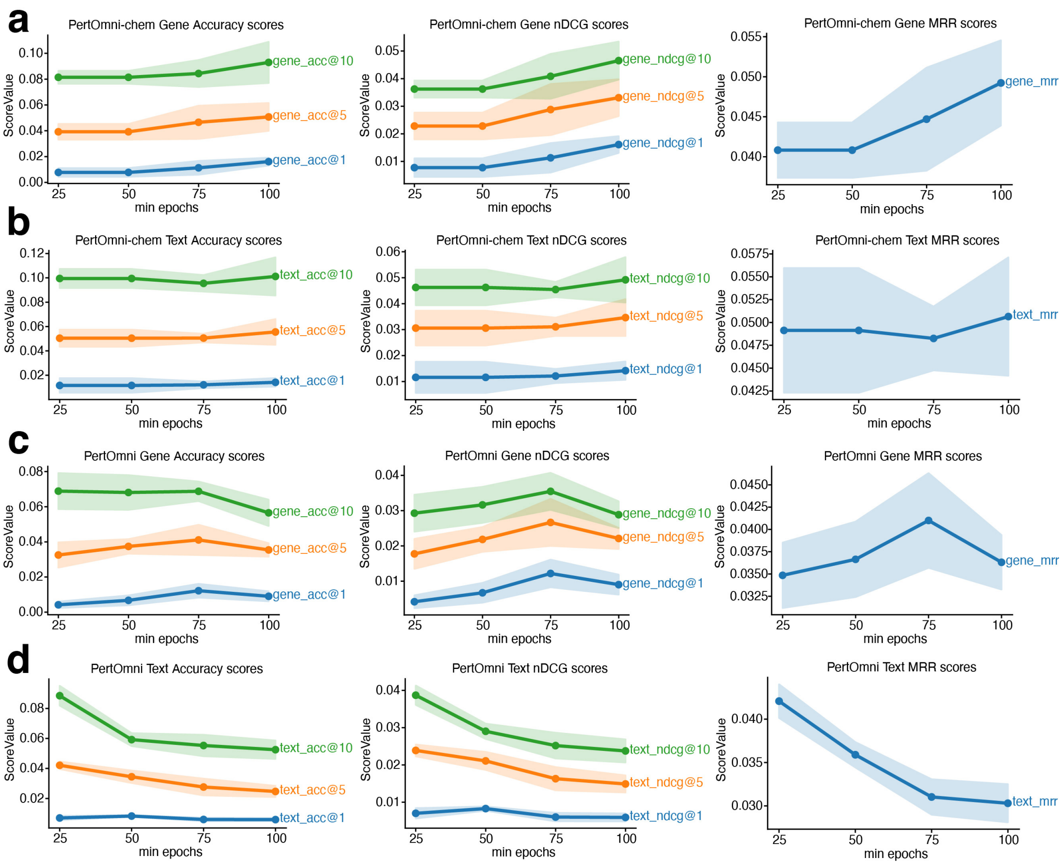

Supplementary Fig. 6: Results of cross-modality retrieval under different minimum epochs settings in Tahoe-100m dataset. (a) Gene2Text retrieval metrics comparison for PertOmni-chem. (b) Text2Gene retrieval metrics comparison for PertOmni-chem. (c) Gene2Text retrieval metrics comparison for PertOmni. (d) Text2Gene retrieval metrics comparison for PertOmni.

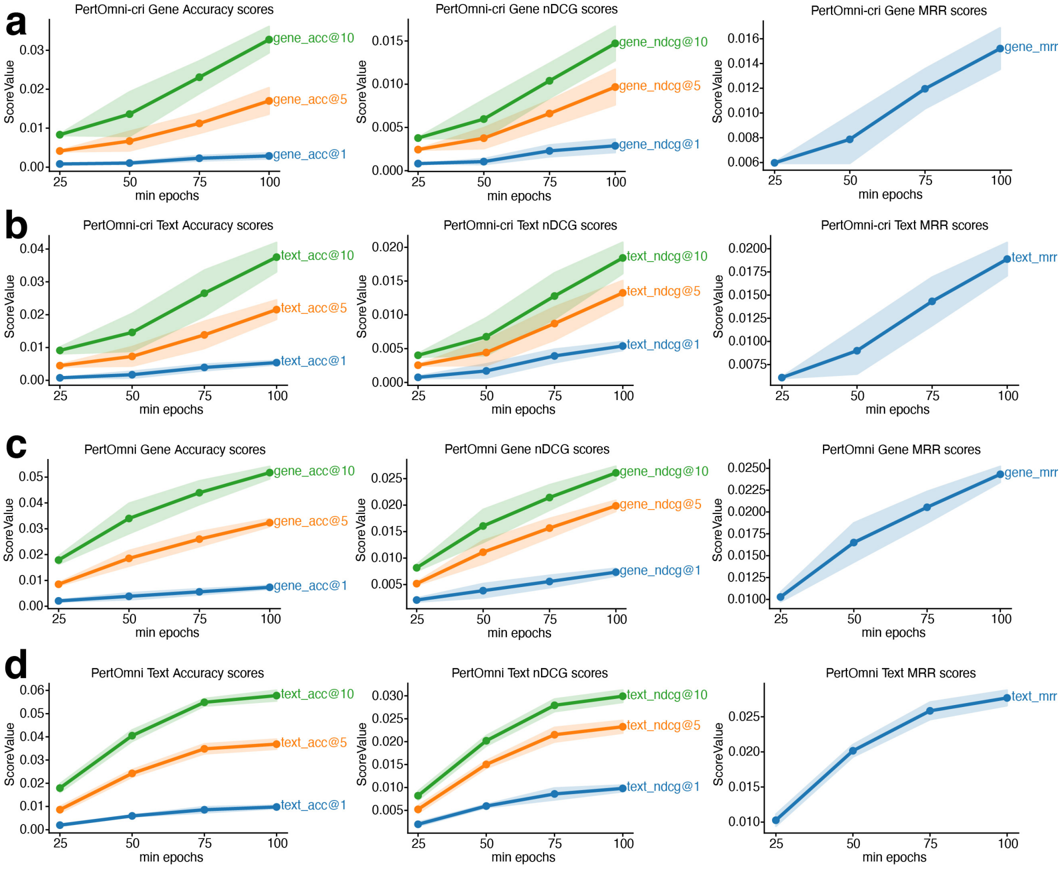

Supplementary Fig. 7: Results of cross-modality retrieval under different minimum epochs settings in the CRISPR dataset. (a) Gene2Text retrieval metrics comparison for PertOmni-cri. (b) Text2Gene retrieval metrics comparison for PertOmni-cri. (c) Gene2Text retrieval metrics comparison for PertOmni. (d) Text2Gene retrieval metrics comparison for PertOmni.

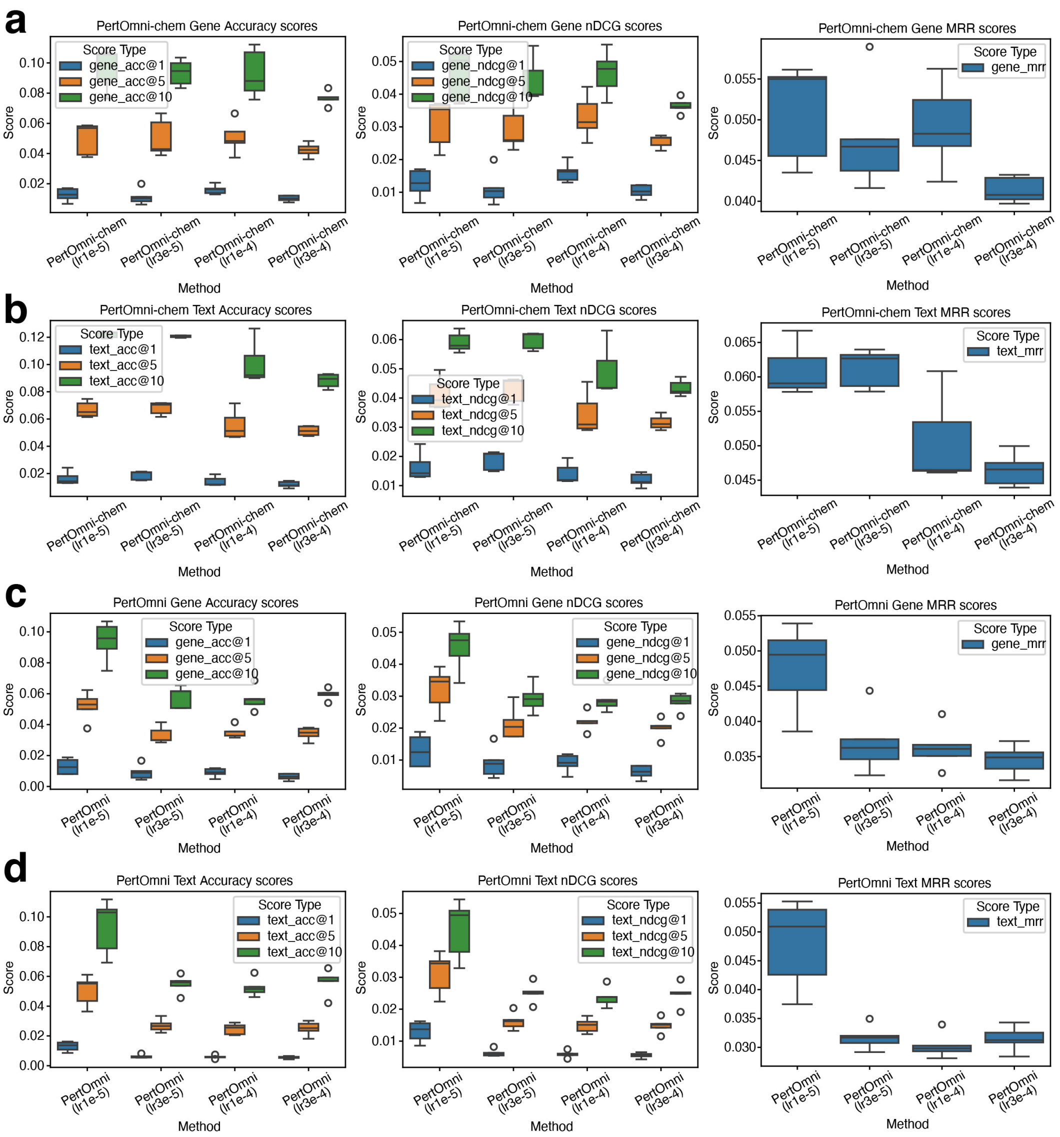

Supplementary Fig. 8: Results of cross-modality retrieval under different learning rate settings in Tahoe-100m dataset. (a) Gene2Text retrieval metrics comparison for PertOmni-chem. (b) Text2Gene retrieval metrics comparison for PertOmni-chem. (c) Gene2Text retrieval metrics comparison for PertOmni. (d) Text2Gene retrieval metrics comparison for PertOmni.

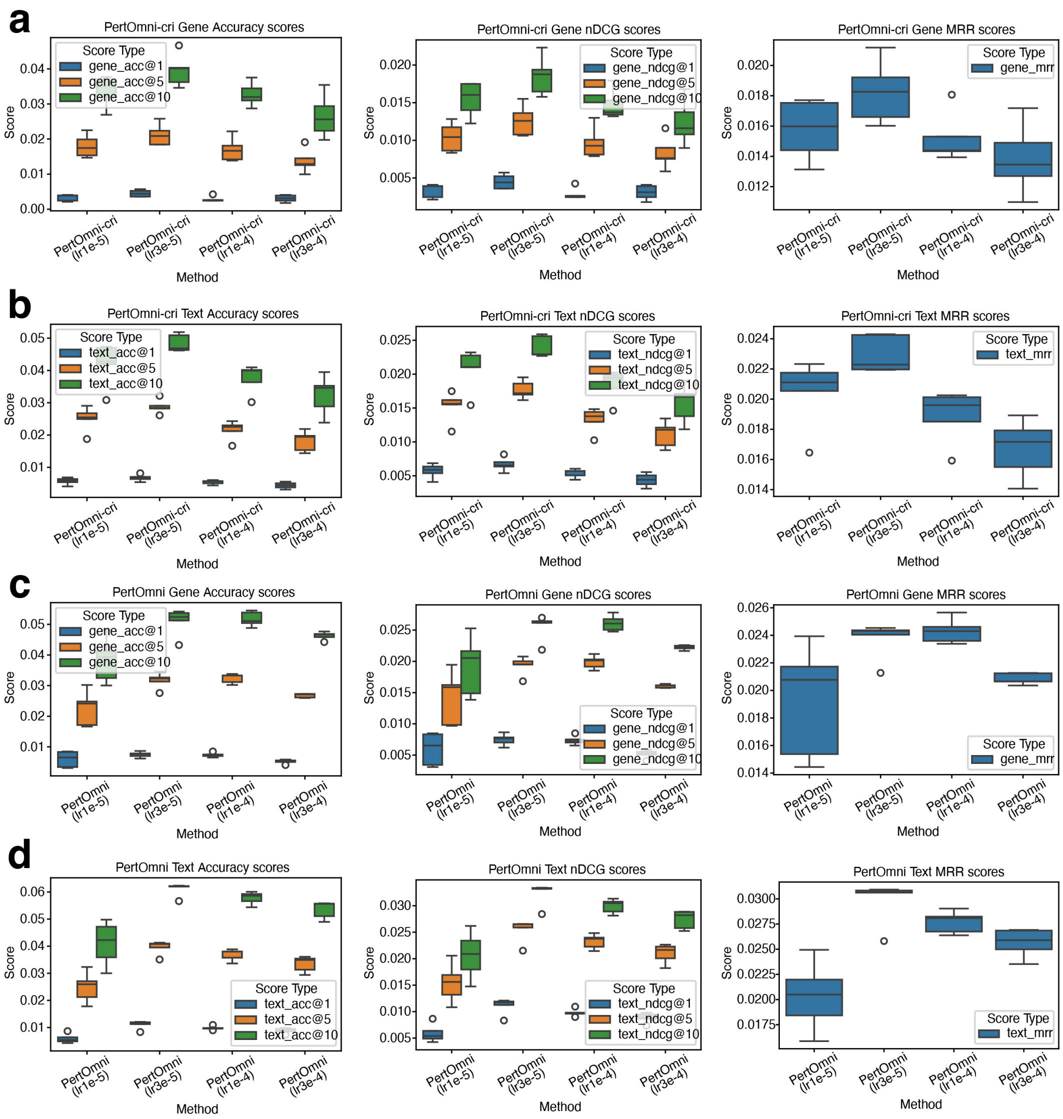

Supplementary Fig. 9: Results of cross-modality retrieval under different learning rate settings in the CRISPR dataset. (a) Gene2Text retrieval metrics comparison for PertOmni-cri. (b) Text2Gene retrieval metrics comparison for PertOmni-cri. (c) Gene2Text retrieval metrics comparison for PertOmni. (d) Text2Gene retrieval metrics comparison for PertOmni.

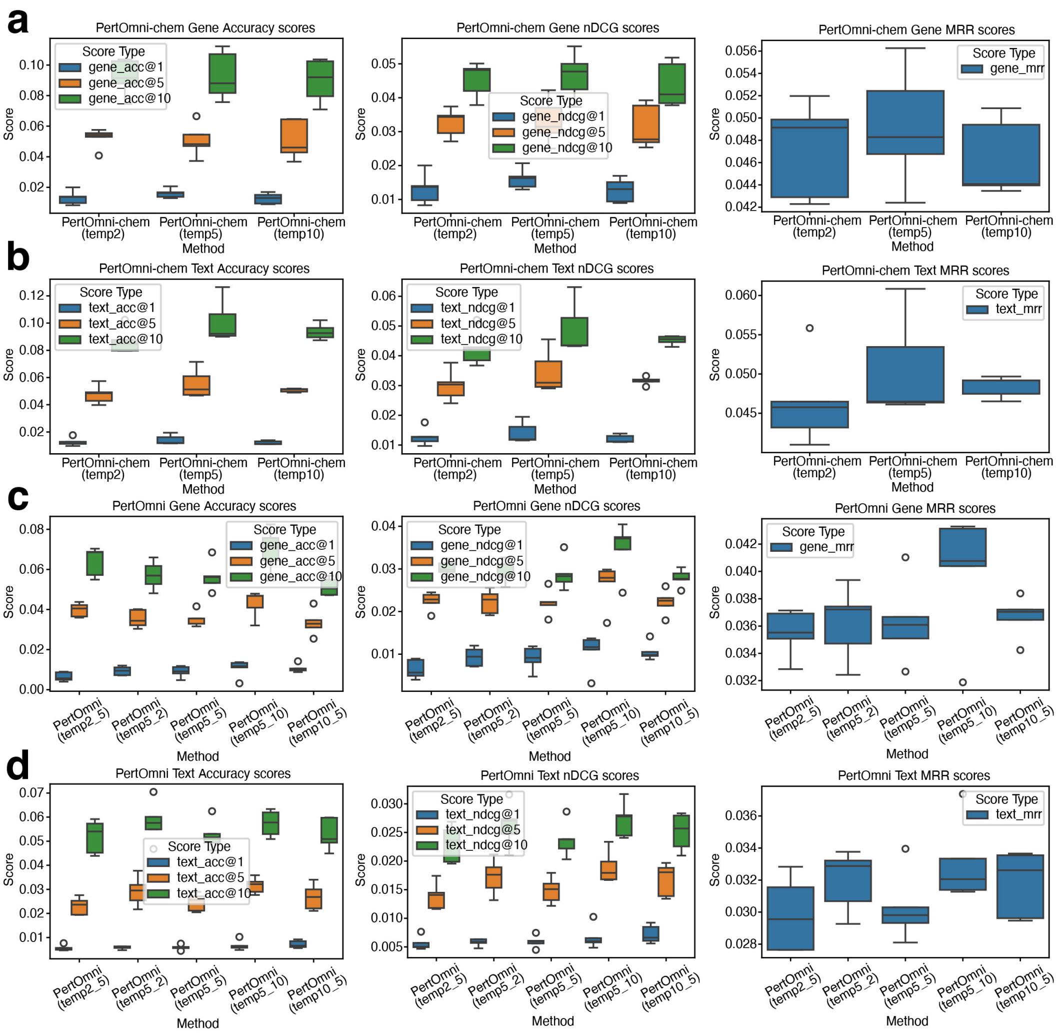

Supplementary Fig. 10: Results of cross-modality retrieval under different temperature settings in the Tahoe-100m dataset. (a) Gene2Text retrieval metrics comparison for PertOmni-chem. (b) Text2Gene retrieval metrics comparison for PertOmni-chem. (c) Gene2Text retrieval metrics comparison for PertOmni. (d) Text2Gene retrieval metrics comparison for PertOmni.

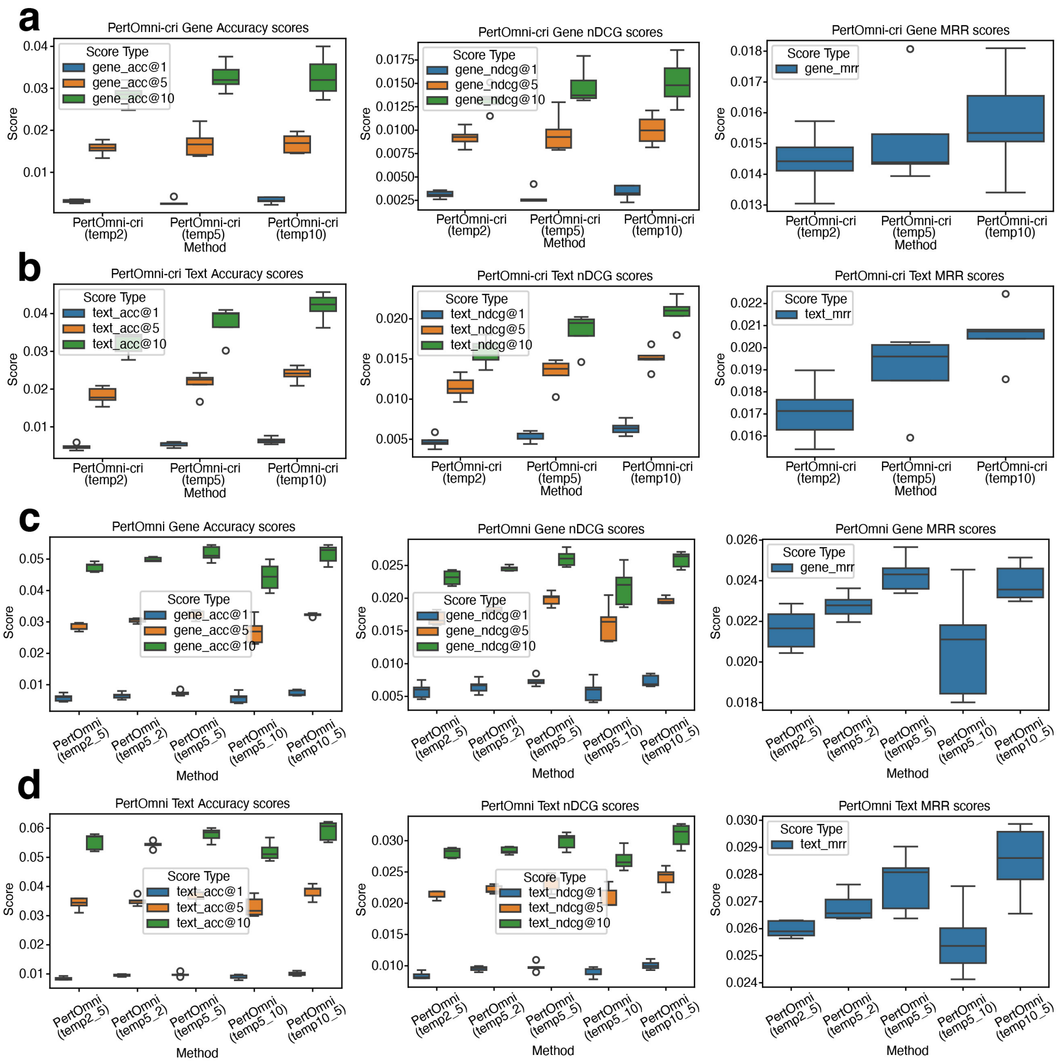

Supplementary Fig. 11: Results of cross-modality retrieval under different temperature settings in the CRISPR dataset. (a) Gene2Text retrieval metrics comparison for PertOmni-cri. (b) Text2Gene retrieval metrics comparison for PertOmni-cri. (c) Gene2Text retrieval metrics comparison for PertOmni. (d) Text2Gene retrieval metrics comparison for PertOmni.

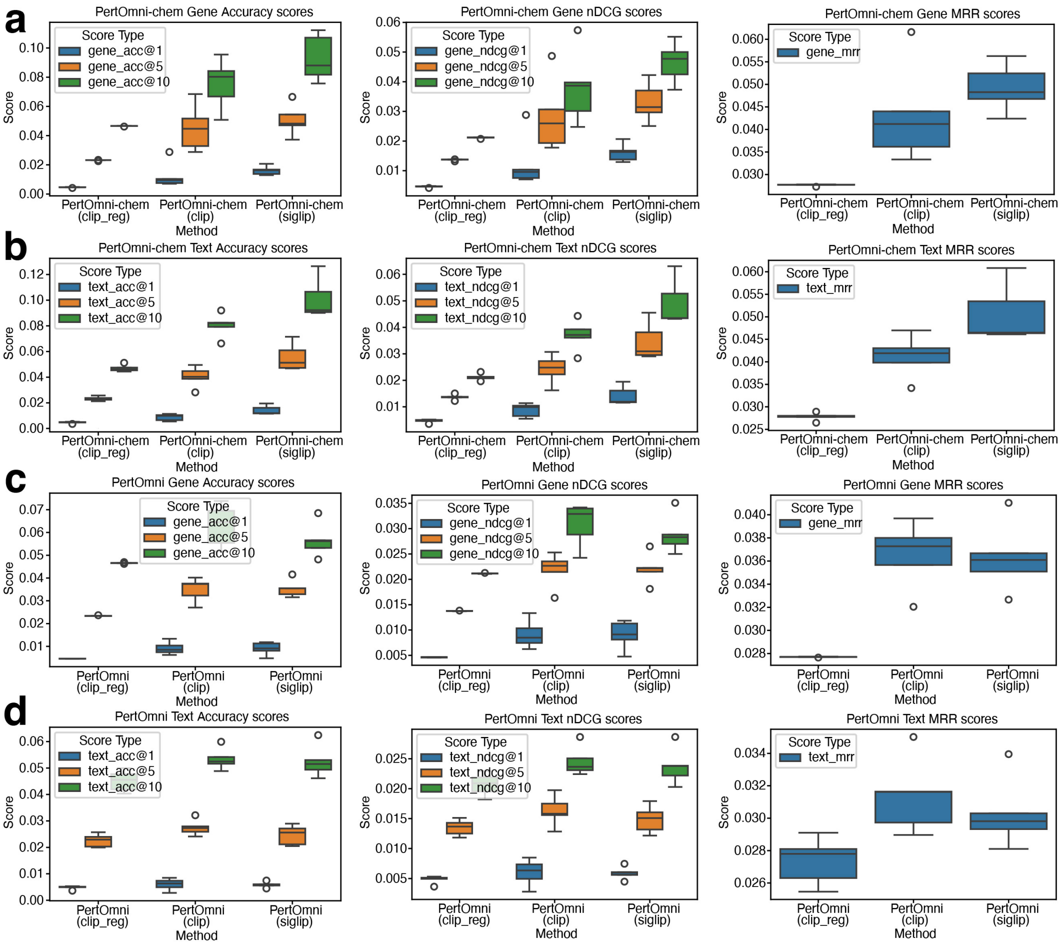

Supplementary Fig. 12: Results of cross-modality retrieval under different loss functions in the Tahoe-100m dataset. (a) Gene2Text retrieval metrics comparison for PertOmni-chem. (b) Text2Gene retrieval metrics comparison for PertOmni-chem. (c) Gene2Text retrieval metrics comparison for PertOmni. (d) Text2Gene retrieval metrics comparison for PertOmni.

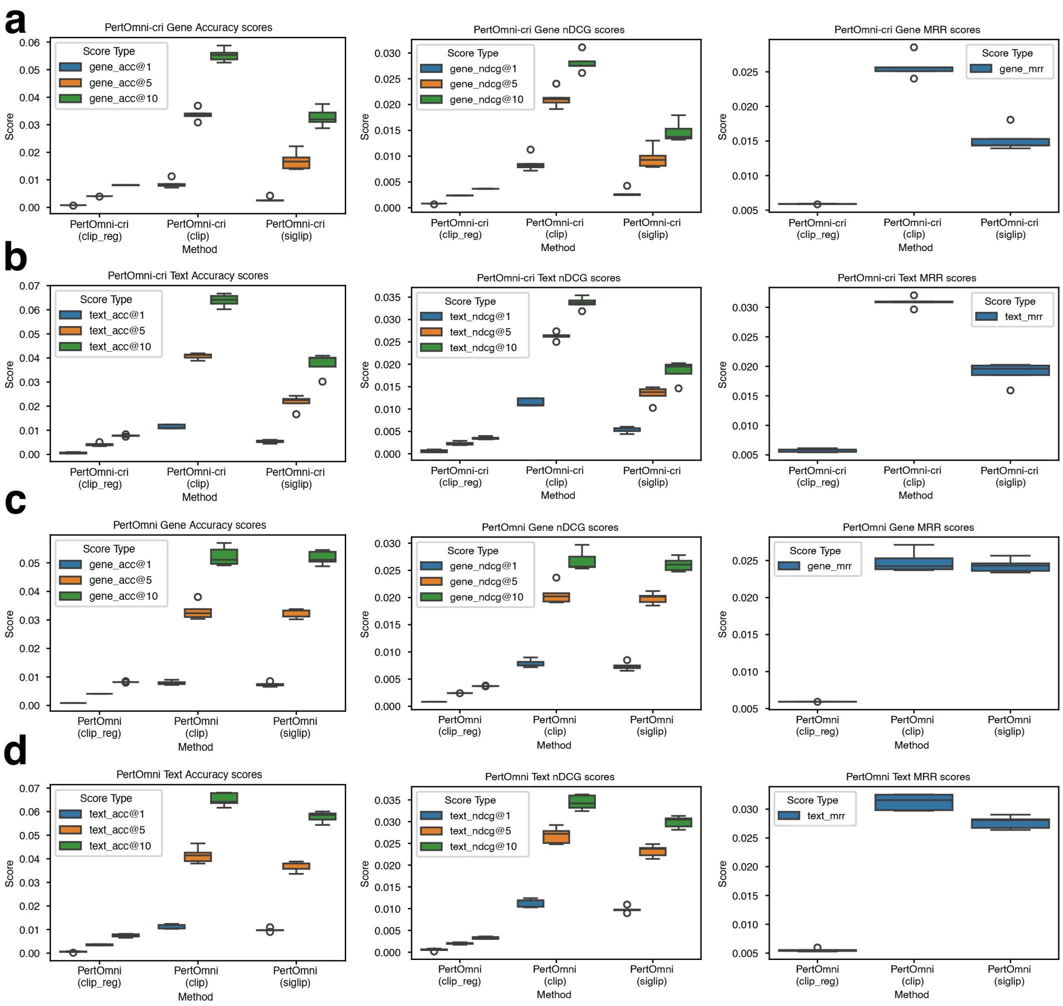

Supplementary Fig. 13: Results of cross-modality retrieval under different loss functions in the CRISPR dataset. (a) Gene2Text retrieval metrics comparison for PertOmni-cri. (b) Text2Gene retrieval metrics comparison for PertOmni-cri. (c) Gene2Text retrieval metrics comparison for PertOmni. (d) Text2Gene retrieval metrics comparison for PertOmni.